

ELECTROMAGNETIC DESIGN BASED ON HYBRID ANALYTICAL AND 3-D FINITE ELEMENT METHOD FOR NOVEL TWO LAYERS BLDC MACHINE

Hassan M. Cheshmehbeigi*, Ebrahim Afjei,
and Behnaz Nasiri

Department of Electrical and Computer Engineering, Shahid Beheshti University G.C., Tehran, Iran

Abstract—This paper deals with electromagnetic design and three-dimensional (3-D) magnetic field analysis of a novel configuration brushless DC (BLDC) field assisted machine based on a hybrid analytical and 3-D finite element method (FEM) analysis. The aim of this hybrid design method is improving the accuracy and computation time for presented complex magnetic structure. In this hybrid design methodology obtained primary magnetic and electric characteristics including magnetic flux density, flux linkage and induced Back-EMF profile for studied configuration are verified by 3-D FE computation. Comparison of the calculated magnetic field and terminal voltage characteristics by their requested values and obtained values illustrates the conformity of the designed parameters. In this study in order to determine the optimum operation, geometry parameters of the proposed machine are optimized based on multi-objective optimization design and genetic algorithm, and finally 3-D FEM verification is coupled by boundary integral equation method (BIEM). Additionally, the accuracy of 3-D FE analysis is verified by comparing the calculated results with the experimental measured values.

1. INTRODUCTION

The BLDC machines are increasingly used in various domestic and in a wide variety of industrial applications for a number of reasons. They are used extensively due to the simple construction, high efficiency, high power density and high reliability. BLDC machines are used in industries for different applications such as home appliances

Received 13 November 2012, Accepted 5 January 2013, Scheduled 17 January 2013

* Corresponding author: Hassan Moradi Cheshmehbeigi (hmch1580@yahoo.com).

automotive, starter generators integrated within engines and turbine spools, generators for wind turbines, aerospace, and servo systems and low-power drive systems [1, 2]. Uncontrollability of the air gap magnetic flux due to the fixed excitation provided by the permanent magnet (PM) and limited operating-speed range are the main disadvantages of permanent magnet BLDC machines for variable speed applications [3, 4].

Numerical technique such as FEM is suggested by different researchers for modeling and parameter identification of electrical machines. In Reference [5] a time stepping FEM is performed for modeling, analysis and identifying of the electromagnetic parameters of a healthy and under fault conditions Induction Machines. Reference [6] has presented the design, optimization of an Outer Rotor OR-PMSM based on coupling boundary element method with permeances network. Reference [7] has presented the design and analysis of a DR-FMPM machine for direct-drive applications by using the time-stepping FEM. In Reference [8] two flux-modulated IPM machines with concentrated windings and distributed windings are quantitatively compared by using FEM. Reference [9] presents the characteristic analysis and performance evaluation of different type portable electric generators for agricultural application. Evaluation of the design parameters and prediction of the transient performance of a novel axial-flux permanent-magnet (AFPM) motor by using 3-D magnetic field analysis utilizing FEM are presented in [10]. References [11, 12] describe the design and analysis of different configuration electrical machines based of finite element analysis.

This paper deals with electromagnetic design and 3-D magnetic field analysis of a novel configuration BLDC field assisted machine based on a hybrid analytical and 3-D FEM analysis. Section 2 of the paper focuses on the principle of operation and structure of the presented BLDC machine. Section 3 describes numerical analysis of magnetic field and FE analysis formulation. Next sections describe analytical analysis, optimization and methodology of evaluation and discussion. Detailed experimental results on the prototype are presented in section 8. Finally, conclusion is presented.

2. NOVEL STRUCTURE AND PRINCIPLE OPERATION

The proposed configuration has double salient poles in both of stator and rotor. Stator has two dependent layers configuration with nine salient poles with concentrated winding. Two stator layers are connected as magnetically and physically with four axially stacked laminations, which are situated on four side of the stator. These axially

stacked laminations pass magnetic flux from one stator set to another side.

The main fluxes in this machine will be produced by DC excited by an assisted field coil which is situated between two stator sets. It should be mentioned that the main flux through the machine can be controlled by regulating the excitation field current. Rotor in this configuration has six salient poles. Also for providing axially flux path through the rotor and closed path for flux through the whole of structure, six axially stacked laminations are considered which are placed in rotor. Figure 1(a) shows the one-phase assembly of proposed machine without phase winding. In this figure, flux path is indicated by arrow. There are two possible winding configurations, shown in Figure 1(b) and (c). Series winding is employed in this studies, in which each phase consists of three series coils (A, A', A''; B, B', B''; C, C', C''). Figure 2(a) shows the cut view of rotor assembly and axially laminated flux path for pass flux troughs rotor. Magnetic flux is leaving the stator in one side, while at the other it is entering. Complete assembly of one pole of

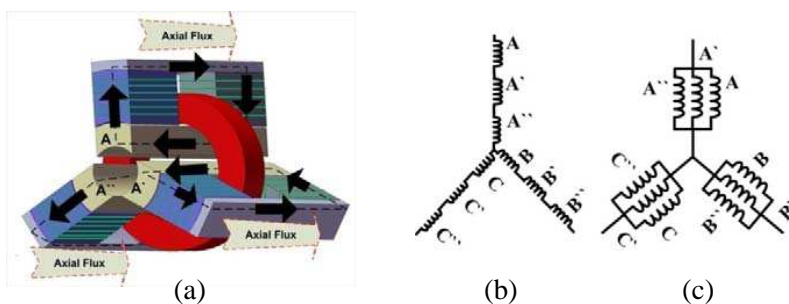


Figure 1. (a) The one-phase assembly of proposed machine without phase winding. (b) (c) Two possible winding configurations.

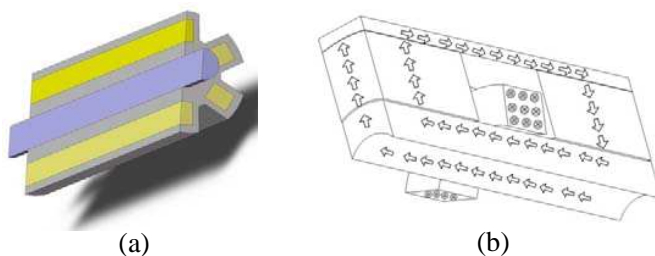


Figure 2. (a) The rotor assembly and axially laminated flux path. (b) Main flux path.

the proposed configuration considering of phase coils and flux path is presented in Figure 2(b).

3. NUMERICAL ANALYSIS OF MAGNETIC FIELD FOR BLDC MACHINE

In this study 3-D FEM is utilized for calculation and analysis of electromagnetic field in and around the proposed configuration. In this paper, the variational energy minimization technique, known as T - Ω formulation, is employed for solving magnetic field problems [13].

$$\nabla \cdot T - \nabla(\nabla\Omega) = 0 \quad (1)$$

$$\nabla^2 T - \mu\sigma \left(\frac{\partial T}{\partial t} \right) = -\mu\sigma \nabla \left(\frac{\partial \Omega}{\partial t} \right) \quad (2)$$

and

$$\nabla^2 \Omega = 0 \quad (3)$$

where T is electric vector potential and Ω is magnetic scalar potential, and which T and Ω are defined by $j = \nabla \times T$ and $H = T - \nabla\Omega$. The detailed derivation was presented in [13].

4. ANALYTICAL ANALYSIS

The stator teeth's flux in the proposed configuration can be expressed as:

$$\varphi_{ts} = \varphi_{\max} \sin \omega t \quad (4)$$

where " φ_{ts} " is the teeth magnetic flux. In this configuration, the frequency of stator teeth's flux can be described as follow:

$$\omega = 2\pi f \xrightarrow{f=N \times Nr} \omega = 2\pi N N r \quad (5)$$

where N is the rated speed in *rps* and Nr the number of rotor teethes. In the iron along the main flux contour B_t can be described as follow [1, 2]:

$$B_t = \mu H_t \left(1 + \frac{\mu |H_t|}{B_{sat}} \right)^{-1} + \mu_0 H_t \quad (6)$$

The iron is characterized by two parameters μ and B_{sat} . In the aligned position, the flux consists of the main flux under two poles and the leakage flux beside the poles as follow:

$$\lambda_{main}(\theta, I_{ph}) = \frac{\theta \lambda_0 R_{si}}{L_g + \frac{L_g^2}{h_r + h_s}} \left[I_{coil} + \frac{2L_g I_{coil}}{h_r + h_s} + \frac{l_{m1} B_{Sat}}{\mu \alpha N_{coil}} - (\xi_{main})^{0.5} \right] \quad (7)$$

$$\lambda_f(\theta, I_{ph}) = \frac{\lambda_0 (\beta_s - \theta R_{si})}{g_f} \left[I_{coil} + \frac{2I_{coil} g_f}{h_r + h_s} + \frac{l_{f1} B_{Sat}}{\mu \alpha N_{coil}} - (\xi_f)^{0.5} \right] \quad (8)$$

$$\xi_{main} = \left(\frac{l_{m1} B_{Sat}}{\mu \alpha N_{coil}} \right)^2 + \frac{2l_{m2} B_{Sat}}{\mu \alpha N_{coil}} I_{coil} + I_{coil}^2 \quad (9)$$

$$\xi_f = \left(\frac{l_{f1} B_{Sat}}{\mu \alpha N_{coil}} \right)^2 + \frac{2\alpha^2 l_{f2} B_{Sat} I_{coil}}{\mu \alpha N_{coil}} + I_{coil}^2 \quad (10)$$

where L_g is air gap length; h_r , h_s are rotor and stator pole height; l_r , l_s are rotor and stator slot width; I_{coil} is coil current; α is number of pole winding in parallel; l_{r1} , l_{r2} are left and right distance between rotor and stator poles; l_{m1} , l_{m2} are main and fringing flux path lengths, respectively. As mentioned before, φ_{max} will occur in saturation condition, then $\varphi_{max} = \varphi_{sat}$ and also $B_{max} = B_{sat}$. By considering the ω , the variation of the flux linkage with rotor position can be expressed as:

$$\varphi_{ts} = \varphi_{sat} \sin(2\pi N N r) t = \left(B_{sat} \frac{D_r}{2} \beta_s L_{st} \right) \sin(2\pi N N r) t \quad (11)$$

Induced EMF is obtained based on Faraday's law. By using Equations (11) and (5), the EMF induced on the coil can be found as:

$$e_{coil} = -N_{coil} \frac{d\varphi_{ts}}{dt} = -N_{coil} \varphi_{max} \omega \cos \omega t \quad (12)$$

$$e_{coil}(\theta_i) = -N_{coil} \omega \frac{\varphi_{ts}(\theta_{i+1}) - \varphi_{ts}(\theta_i)}{\Delta \theta} \quad (13)$$

It shows that induced EMF on the coil depends on the number of coil turns and time derivation of stator teeth magnetic flux. Finally, rms value of Back-EMF can be found as:

$$E_{rms_{coil}} = 2\pi N N r N_{coil} \frac{\varphi_{max}}{\sqrt{2}} = \frac{\pi \sqrt{2}}{2} B_{sat} N N r D_r L_{st} \beta_s N_{coil} \quad (14)$$

where β_s , β_r are stator and rotor pole arc respectively; L_{st} is motor length; θ is rotor position; B_{sat} is saturation flux density. Induced EMF in a coil with " N_{coil} " turns for proposed configuration is expressed by Equation (14) which shows that distributed magnetic flux density waveform and induced waveform in each phase coil are similar in shape with respect to position around the rotor. Figure 3 shows different possible winding configurations for obtaining different desired terminal voltages. Obtained flux linkage verses rotor angle from analytical analysis are presented in Figure 4. As shown in Figure 4, flux linkages in aligned positions for field currents 1 A, 3 A and 5 A are 51 mWb, 67 mWb and 86 mWb, respectively.

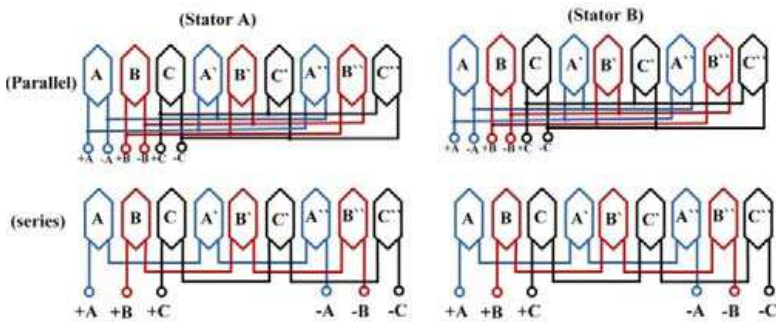


Figure 3. Winding connection diagram for one side of proposed machine.

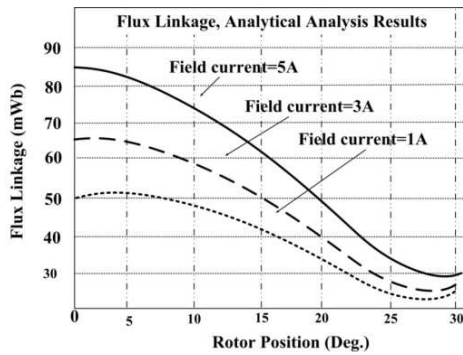


Figure 4. Flux linkage versus rotor position from analytical analysis.

And also for unaligned positions, these values are 16 mWb, 20 mWb and 31 mWb, respectively. Obtained induced EMF based on Faraday’s law expressed by Equation (14) and flux linkage for different rotor angles and two different field currents 1 A and 5 A are presented in Table 1.

5. SIMULATION RESULTS

To evaluate the accuracy of design procedure and performance of the proposed configuration 3-D FEM is performed. Figure 5(a) shows the DC excited assisted field coil as main MMF source. As shown in Figure 5(b), the main fluxes in this machine will be produced by DC excited field coil situated between two stator sets. Figure 5(c) shows the magnetic flux density arrows for axially laminated path in rotor.

Table 1. Flux linkage and induced back-EMF analytical analysis results.

Rotor Angle (Deg.)	Analytical Analysis Results			
	Field Current = 1 A		Field Current = 5 A	
	Flux Linkage (Wb)	Induced Back-EMF (V)	Flux Linkage (Wb)	Induced Back-EMF (V)
0	0.016	0.014	0.0306	0.034
4	0.0163	3.356	0.0319	9.156
8	0.0311	5.758	0.0411	16.124
12	0.0383	8.452	0.0486	24.321
16	0.0450	11.354	0.0631	32.025
20	0.0479	6.785	0.0731	20.021
24	0.0490	4.279	0.0814	11.187
28	0.0516	1.496	0.0544	5.149

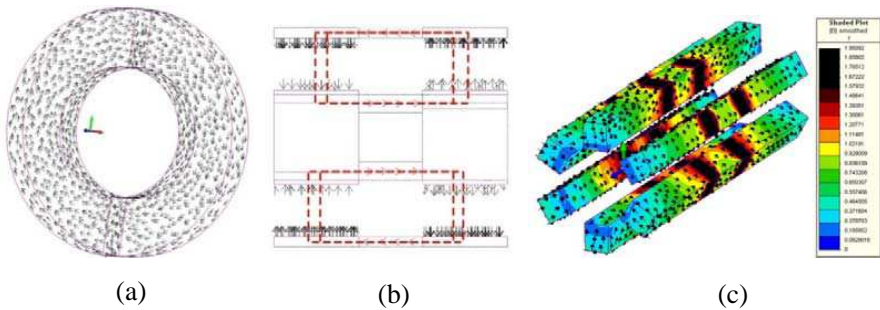


Figure 5. Magnetic flux density arrows for different parts of the proposed machine.

Figure 5 also shows that the magnetic flux passes through the axially laminated rotor flux paths along the length of the rotor. The amplitude of the magnetic flux density is 1.6 Tesla which approves operation of the studied structure in saturation region. Results of computed flux linkage of 3-D magnetic field in the proposed machine for different rotor positions are presented in Figure 6(a). The obtained results in Figure 6(a) are related to field currents 1 A, 3 A and 5 A. As shown in Figure 6(a), flux linkages in aligned positions for field currents 1 A, 3 A and 5 A are 49 mWb, 64 mWb and 85 mWb, respectively. And

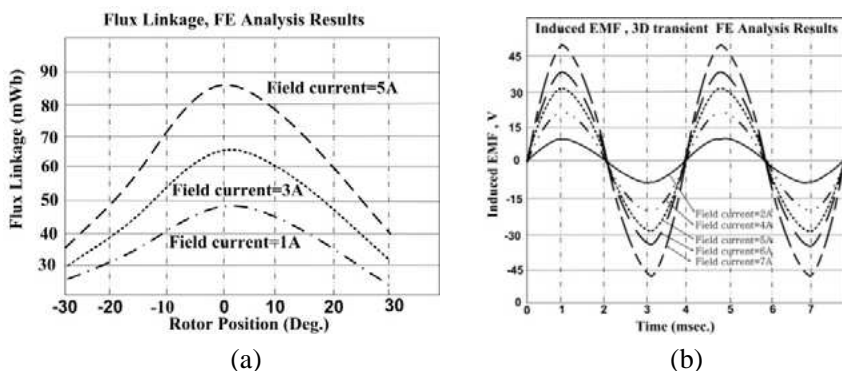


Figure 6. (a) Computed flux linkage for different rotor positions. (b) Computed induced Back-EMF from 3-D FE analysis for different rotor angles.

Table 2. Induced back-EMF for different speeds.

Speed (R.P.M)	No Load	
	$I_{\text{Field}} = 2 \text{ A}$	$I_{\text{Field}} = 3 \text{ A}$
	Out Put Voltage (v)	Out Put Voltage (v)
1000	10.2	12.3
1500	12.3	14.1
2000	16.1	18.2
2500	24.5	26.3
3000	32.3	35.5
3500	40.1	46.2
4000	45.4	53.1

also for unaligned positions these values are 14 mWb, 30 mWb and 36 mWb, respectively. Computed induced Back-EMF from 3-D FE analyses for different rotor angles and six different field currents 2 A, 4 A, 5 A, 6 A and 7 A are presented in Figure 6(b). From transient FE analysis, induced Back-EMF for different speeds from 1000 rpm to 4000 rpm under two field currents 2 A and 3 A are presented in Table 2. As shown in Table 2, maximum back-EMF will occur in speed 4000 rpm and field current 3 A. Obtained results show that output voltage can be regulated by controlling the field current, which means that it is possible to control the machine's main flux by regulating the excitation current.

6. HYBRID MAGNETIC OPTIMIZED DESIGN METHODOLOGY

Hybrid design method employing 3-D FE analysis and analytical method will improve the accuracy and computation time of design complex magnetic structure. At first, an analytical method capable of calculating, with acceptable accuracy, flux distribution and terminal induced EMF characteristics, is applied to obtain the initial machine dimension, and the desired parameters before FEA is applied to complex magnetic axial flux path. In the second step, primary magnetic and electric characteristics of studied configuration obtained from analytical analysis step are verified by 3-D FE computation, and the initial machine dimensions are indicated for being applied to optimization procedure. Finally, multi-objective optimization design and genetic algorithm have been utilized for optimizing the machine

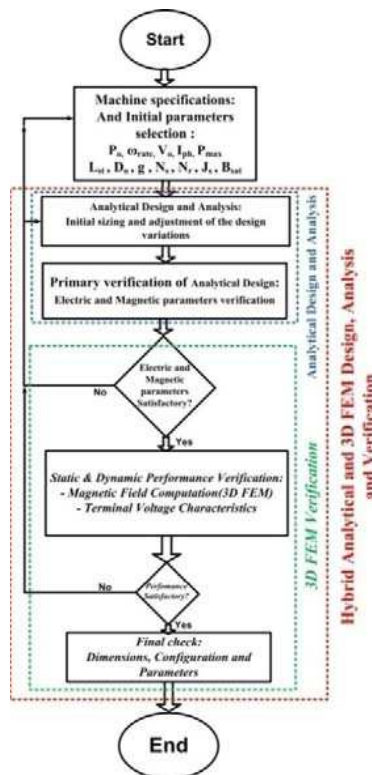


Figure 7. Algorithm of design process.

Table 3. The constraints, initials and optimal variables values.

Design Variables	Constraints	Initial value	Optimal value
L_{st}	$130 \leq X \leq 155$	146	(mm)
β_s	$28 \leq X \leq 32$	30	(Deg.)
D_r	$65 \leq X \leq 74$	70	(mm)
H_s	$20 \leq X \leq 36$	30	(mm)
D_o	$133 \leq X \leq 150$	145	(mm)
W_f	$2.7 \leq X \leq 1.5$	2	(mm)

geometers. $\vec{x} = [x_1, x_2, \dots, x_D]$, $\vec{x} \in R^D$ and $F = \{g_j(\vec{x}) \leq 0, j = 1, \dots, m\}$ as design parameters, $x_i^L \leq x_i \leq x_i^U, i = 1, \dots, D$ as the boundary of the parameters and $f(\vec{x}) = [f_1(\vec{x}), f_2(\vec{x}), \dots, f_k(\vec{x})]$ as the objective function set will describe multi-objective nonlinear optimization problem in this optimal design problem [6]. It should be mentioned that in this work, Genetic Algorithm is utilized to solve the multi-objective problem. The objectives functions are selected to decrease Iron losses and increase developed power. The stack length, axial path flux, stator teeth width, bore and stator diameter, stator teeth height and field winding window of proposed configuration are also selected as the design variables. The constraints, initial and optimal values in the design variables are given in Table 3. In this work, finally, the machine performance is evaluated from the 3-D finite element results. During each iteration of the minimization process, the equivalent circuit parameters are extracted from an iterative finite element method. The objective function and desired constraints are replaced with approximations by means of least squares fitting. The algorithm of design procedure is shown in Figure 7.

7. METHODOLOGY EVALUATION FOR FLUX DENSITY DISTRIBUTION

The BIE method permits formulation of field variables along the boundaries, and FE technique gives precise information of the machine parameters using machine geometry, dimensions, and materials. Therefore, a hybrid computational methodology based on coupling the FE and BIE for the calculation of the magnetic field can be very efficient to confirm the accuracy of the 3-D FE analysis simulation results. The contribution of all boundary elements to the magnetic field at a given point $k = (x_k, y_k, z_k)$, in terms of the magnetic vector

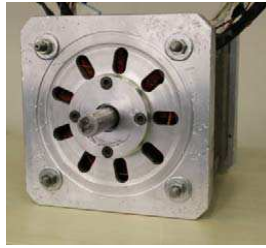


Figure 8. Proposed BLDC generator fabricated in the laboratory.

potential, is given by the following relationship [14, 15]:

$$C_k A_k = \sum_{\epsilon} \int_{\Gamma_{\epsilon}} \left(G \frac{\partial A}{\partial n} - A \frac{\partial G}{\partial n} \right) d\Gamma_{\epsilon} \quad (15)$$

where

$$G = \frac{1}{2\pi} L n \frac{1}{r} \quad (16)$$

G is a Green's function and r the distance from the given point $k = (x_k, y_k, z_k)$ to a current point (x, y, z) on the airgap boundary. The coupling of the FE and BIE formulations is done by expressing the continuities of the magnetic vector potential and of the tangential component of the magnetic field on the airgap interfaces. The consideration of the Dirichlet boundary condition on the external stator outline leads to a nonlinear system of equations solved using the Newton-Raphson algorithm [16, 17]. The hybrid coupling method is applied to the calculation of the magnetic field in the proposed BLDC machine, and the obtained results for magnetic field in aligned, unaligned and half-aligned are 0.974, 0.357, and 0.687 Tesla, respectively. The results obtained by the hybrid coupling method are compared with those based on 3-D FEM, which show 2.40%, 9.50% and 1.50% tolerance for aligned, un-aligned and half-aligned positions, respectively, indicating an excellent conformity.

8. EXPERIMENTAL RESULTS

In order to evaluate the accuracy of the results obtained from the 3-D finite element field computation, a simple experimental machine was built and tested (Figure 8). This machine has three-phases and field assisted structure. Dimensions are: stator outer diameter is 145 mm; rotor outer diameter is 70 mm; number of rotor teeth is 6; number of stator teeth is 9; rotor pole angle is 30 Deg.; stator pole angle is 30 Deg.;

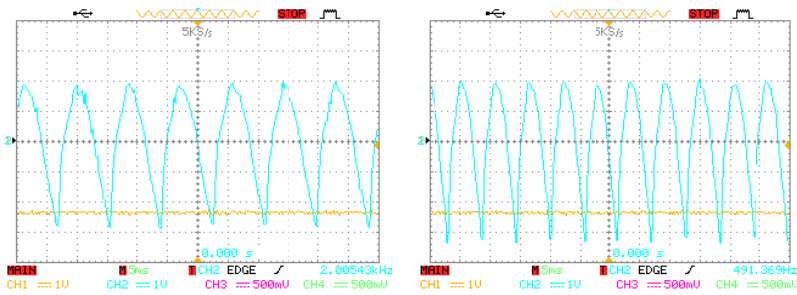


Figure 9. The actual output voltage of 3 phases for two different field currents equal to 0.5 A, 1 A and two different speeds 1500 rpm, 2000 rpm.

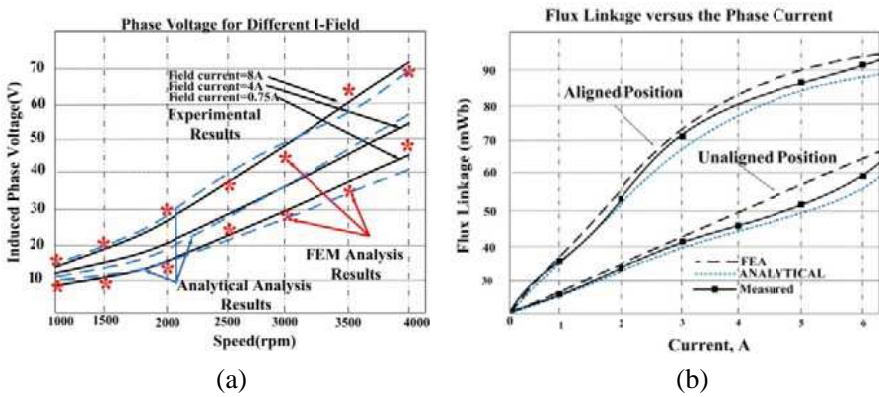


Figure 10. (a) Comparison of FEM results and experimentally results. (a) Flux linkages vs. current characteristics.

air gap length is 146 mm; number of turns per phase is 40 turns; rated speed is 3600 rpm; rated power is 1500 w.

In experimental test, the shaft of the machine is connected to a motor to act as a prime mover. Output parameters of generator are measured for No-Load and under load by different speeds from 1000 rpm up to 4000 rpm. All these measurements are done for different field currents equal to 0.75 A, 4 A and 8 A. The actual output voltage of 3-phases for two different field currents equal to 0.5 A, 1 A, and two different speeds 1500 rpm, 2000 rpm are also shown in Figure 9. The voltages have harmonic due to the shape of the stator and rotor poles and local saturation.

The results of these tests and comparison with those obtained from

Table 4. Comparison of the field assisted BLDC machine and the PM excited machine.

Field assisted BLDC Machine	PM excited Machine
<ul style="list-style-type: none"> - Regulating the terminal voltage by controlling the magnetizing field current - Operating in a Wide Speed Range - Operating in a Wide temperature Range - Need to simple power electronic solutions for regulating terminal voltage 	<ul style="list-style-type: none"> -Limited operating-speed range - limited operating temperature range - Lacks field control - cost - demagnetization - need to power electronic solutions for regulating terminal voltage,

analytical analysis and FEM analysis are shown in Figure 10(a). In these figures, curve fitting has been used for better presentation of the data points. As shown in Figure 10(a), induced peak to peak output voltages for different speeds in No-Load mode are plotted.

Maximum voltage is obtained in speed 4000 rpm and field current 8 A. Presented results show that the amplitude of generated voltage is dependent on shaft speed and value of field current. The flux linkage-current characteristics obtained by analytical model, FEM model and measuring results are presented in Figure 10(b). Measuring results are in good agreement with those obtained by the theoretical approach based on FEM simulation in Section 5. For verification of 3D computed magnetic flux and analytical results in different parts of the prototype machine, flux density measurement in the teeth of the motor is carried out by GAUSSMETER BROCKHOUSE 460. Obtained results for measured flux density in aligned and un-aligned positions are 1.0119 and 0.3633 Tesla, respectively. Measured results are in good agreement with those obtained by the theoretical approach based on FEM simulation in Section 5. Table 4 shows the comparison between field assisted BLDC machine and the PM excited machine.

9. CONCLUSION

This paper deals with a hybrid analytical and 3-D magnetic FEM, design-analysis and verification procedure for novel configuration of BLDC field assisted machine. Aid of this hybrid design method is improving the accuracy and computation time for complex magnetic

structure like to presented machine structure. In this hybrid design methodology, obtained primary magnetic and electric characteristics for studied configuration are verified by 3-D FE computation. The proposed configuration has salient poles in both rotor and stator by utilizing 3-phases concentrated windings warped on the stator teetles. The main flux is produced by DC current excitation of an assisted field coil situated between the stator layers. For the presented complex magnetic structure, the magnetic field distribution is numerically computed by 3-D FEM. The primary characteristics of the machine including magnetic flux density, flux linkage and induced Back-EMF profile are obtained. A proto-type BLDC machine has also been built and tested. Additionally, the accuracy of 3-D FE analysis is verified by comparing the calculated results with the experimentally measured values.

REFERENCES

1. Hanselmann, D. C., *Brushless Permanent Magnet Motor Design*, Magna Physics Pub., Jan. 31, 2006.
2. Hendershot, J. R. and T. J. E. Miller, *Design of Brushless Permanent Magnet Machines*, Motor Design Books, LLC, Mar. 30, 2010.
3. Faiz, J. and B. M. Ebrahimi, "Static eccentricity fault diagnosis in an accelerating no-load three-phase saturated squirrel-cage induction motor," *Progress In Electromagnetics Research B*, Vol. 10, 35–54, 2008.
4. Boldea, I., *Variable Speed Generators*, Taylor & Francis Group, 2006.
5. Vaseghi, B., N. Takorabet, and F. Meibody-Tabar, "Transient finite element analysis of induction machines with stator winding turn fault," *Progress In Electromagnetics Research*, Vol. 95, 1–18, 2009.
6. Touati, S., R. Ibtouen, O. Touhami, and A. Djerdir, "Experimental investigation and optimization of permanent magnet motor based on coupling boundary element method with permeances network," *Progress In Electromagnetics Research*, Vol. 111, 71–90, 2011.
7. Liu, C. and K. T. Chau, "Electromagnetic design and analysis of double-rotor flux-modulated permanent-magnet machines," *Progress In Electromagnetics Research*, Vol. 131, 81–97, 2012.
8. Xu, G., L. Jian, W. Gong, and W. Zhao, "Quantitative comparison of flux-modulated interior permanent magnet machines

- with distributed windings and concentrated windings,” *Progress In Electromagnetics Research*, Vol. 129, 109–123, 2012.
9. Norhisam, M., S. Ridzuan, R. N. Firdaus, C. V. Aravind, H. Wakiwaka, and M. Nirei, “Comparative evaluation on power-speed density of portable permanent magnet generators for agricultural application,” *Progress In Electromagnetics Research*, Vol. 129, 345–363, 2012.
 10. Mahmoudi, A., S. Kahourzade, N. A. Rahim, W. P. Hew, and N. F. Ershad, “Slot-less torus solid-rotor-ringed line-start axial-flux permanent-magnet motor,” *Progress In Electromagnetics Research*, Vol. 131, 331–355, 2012.
 11. Mahmoudi, A., S. Kahourzade, N. A. Rahim, and H. W. Ping, “Improvement to performance of solid-rotor-ringed line-start axial-flux permanent-magnet motor,” *Progress In Electromagnetics Research*, Vol. 124, 383–404, 2012.
 12. Mahmoudi, A., N. A. Rahim, and H. W. Ping, “Axial-flux permanent-magnet motor design for electric vehicle direct drive using sizing equation and finite element analysis,” *Progress In Electromagnetics Research*, Vol. 122, 467–496, 2012.
 13. Ren, Z., “ T - Ω formulation for Eddy-current problems in multiply connected regions,” *IEEE Transactions on Magnetics*, Vol. 38, No. 2, 557–560, Mar. 2002.
 14. Hsieh, K.-T., “Hybrid Fe-Be implementation on electromechanical systems with moving conductors,” *IEEE Transactions on Magnetics*, Vol. 43, No. 3, 1131–1133, 2007.
 15. Qiu, Z.-J., J.-D. Xu, G. Wei, and X.-Y. Hou, “An improved time domain finite element-boundary integral scheme for electromagnetic scattering from 3-D objects,” *Progress In Electromagnetics Research*, Vol. 75, 119–135, 2007.
 16. Jian, L., G. Xu, Y. Gong, J. Song, J. Liang, and M. Chang, “Electromagnetic design and analysis of a novel magnetic-gear-integrated wind power generator using time-stepping finite element method,” *Progress In Electromagnetics Research*, Vol. 113, 351–367, 2011.
 17. Liang, J., L. Jian, G. Xu, and Z. Shao, “Analysis of electromagnetic behavior in switched reluctance motor for the application of integrated air conditioner on-board charger system,” *Progress In Electromagnetics Research*, Vol. 124, 347–364, 2012.